Processive translocation of cohesive and non-cohesive cohesin *in vivo*

Running Title: Processive translocation of cohesin

Melinda S. Borrie and Marc R. Gartenberg[1,2]

Department of Biochemistry and Molecular Biology
Robert Wood Johnson Medical School
Rutgers, The State University of New Jersey
Piscataway, NJ 08854

[1]Member of The Rutgers Cancer Institute of New Jersey, New Brunswick, NJ 08901
[2]Correspondence: marc.gartenberg@rutgers.edu

Keywords
cohesin, sister chromatid cohesion and loop extrusion, transcription, Eco1, Wpl1

Abstract

Cohesin is a central architectural element of chromosome structure that regulates numerous DNA-based events. The complex holds sister chromatids together until anaphase onset and organizes individual chromosomal DNAs into loops. *In vitro*, cohesin translocates along DNA and extrudes loops in an ATP-dependent fashion. *In vivo*, cohesin redistributes in response to transcription as if pushed by RNA polymerase. Direct evidence of processive genomic translocation by the complex, however, is lacking. Here, obstacles of increasing size were tethered to DNA in yeast to detect translocation. The obstacles were built from a GFP-lacI core fused to one or more mCherries. Cohesin translocation was initiated from an upstream gene. A chimera with four mCherries blocked cohesin passage in late G1. During M phase, the threshold barrier to passage depended on the state of cohesion: non-cohesive complexes were also blocked by four mCherries whereas cohesive complexes were blocked by only three mCherries. That synthetic barriers alter cohesin redistribution demonstrates that the complex translocates processively on chromatin *in vivo*. The approach provides a relative measure of the maximum size of the protein chamber(s) that embraces DNA during cohesin translocation. The data indicate that the cohesive embrace is more restrictive than the embrace of non-cohesive complexes.

Introduction

Cohesin is a central architectural element of chromosome structure that functions by bringing distant DNA sites together (1). The protein complex was first characterized for its role in sister chromatid cohesion. Cohesin is now known to participate in most if not all fundamental chromosomal processes, including transcription, replication and repair. Recent work has shown that the complex also organizes chromosomes into large DNA loops that contribute to the segmentation of the genome into self-associating domains. Mis-regulation of cohesin has been identified as the cause of certain developmental diseases known collectively as cohesinopathies (2). Mutations in cohesin subunits have also been associated with human cancers.

The evolutionarily conserved core cohesin complex contains two SMC subunits (Smc1 and Smc3) and an α kleisin subunit Mcd1 (also known as Scc1/Rad21), which form a protein ring that can embrace DNA topologically (3). In yeast, the complex accumulates densely across tens of kilobases surrounding centromeres (4, 5). Along chromosome arms, the complex binds between convergently transcribed genes. Chromosome conformation capture (3C) techniques have shown that such sites participate both in sister chromatid cohesion and chromosomal loop formation (6-9). Cohesin performs these same architectural functions in higher eukaryotes (10-12).

Cohesin loading onto yeast chromosomes begins each cell cycle in late G1. Initially, the interaction is dynamic. The complex cycles on and off DNA because loading is balanced by an unloading factor, WAPL (Wpl1 or Rad61 in yeast). During S phase, Eco1 halts cohesin loss by acetylating the Smc3 cohesin subunit, which antagonizes Wpl1 (13-17). Eco1 travels with the DNA replication fork, presumably to couple the stabilization of cohesin complexes directly with the creation of sister chromatids (18).

A second dynamic property of cohesin is the ability to redistribute on chromosomes. Cohesin accumulates at genomic sites that are often great distances from where the complex initially loads (19). RNA polymerase was seen as a central driver of repositioning because cohesin on dormant or weakly transcribed genes was repositioned downstream by transcriptional induction (4, 5, 20). Translocation of complexes by processive movement along the chromatin contour best

81 explains repositioning, particularly given cohesin's topological embrace around DNA. Indeed,
82 cohesin was shown to move along DNA *in vitro*, and transcribing RNA polymerase was shown
83 to bias the directionality of movement (21-23). More recent biochemical work showed that
84 cohesin, in combination with an auxiliary loading factor, possesses an intrinsic motor activity
85 that enables translocation of the complex along naked and nucleosomal DNA in an ATP-
86 dependent fashion (24, 25). Importantly, these studies showed that translocating cohesin can
87 extrude DNA loops, an activity that is thought to form the large chromosomal loops that typify
88 genomes (26-28). In support of the loop extrusion model, the size and distribution of
89 chromosomal loops are altered by factors that influence the residence time of cohesin on
90 chromatin (7, 8, 29-31). However, cohesin complexes have rarely been characterized during the
91 act of translocation *in vi*vo.
92
93 We recently obtained evidence for cohesin translocation on chromosomal DNA in yeast using a
94 system involving transcriptional induction of a cohesin bound gene (32). Upon induction of the
95 gene, cohesion of the locus was lost. If, however, the locus was first converted to an
96 extrachromosomal circle, cohesion persisted. The results are most readily explained by cohesin
97 complexes that redistribute by processive translocation because such complexes cannot migrate
98 off circularized DNA. In the present study, the properties of translocating cohesin complexes
99 were further studied by measuring their ability to bypass synthetic obstacles of increasing
100 molecular size. This work provides direct evidence that cohesin translocates processively on
101 DNA in response to transcription *in vivo*. Moreover, the data reveal that the fate of encounters
102 with barriers depends on the cohesive state of the complex: a barrier sufficient to trap cohesive
103 complexes is not large enough to trap non-cohesive complexes.

Results

Nuclear membrane tethering of DNA blocks cohesin translocation

Our previous study found that DNA circularization, as well as downstream convergently oriented genes, prevented transcription-driven cohesion loss (32). While DNA circles capture complexes that might remain mobile, we inferred that downstream genes act as barriers to cohesin passage. Intriguingly, DNA-bound lac repressors did not behave similarly. We hypothesized that the bacterial protein (lacI fused to GFP) was smaller than the chamber of the complex through which DNA passes. If cohesin truly redistributes by translocation *in vivo*, then DNA-bound proteins of sufficient size should block passage of the complex. To begin to explore this concept, we used a GFP-lacI chimera linked to FFAT, a tetrapeptide motif that associates with the inner nuclear membrane (33). When tethered to DNA and the nuclear membrane simultaneously, GFP-FFAT-lacI essentially represents an immobile obstacle of infinite size (Figure 1A).

Translocation assays were performed on an engineered genomic locus (Figure 1B) that contains the 256 lac operator array downstream of *URA3*, a gene that can be induced 3-5 fold by withholding uracil. Previous work showed that cohesive complexes associate with uninduced *URA3* until transcriptional induction triggers their departure. Cohesin levels at the gene do not diminish, however, because new complexes reload during the experimental interval (32). Here, chromatin immunoprecipitation coupled with quantitative real-time PCR (ChIP-qPCR) was used to monitor arrival of cohesin at a downstream site immediately preceding the lac operator array (hereafter referred to as the 5'lacO site).

URA3 transcription was induced after cells were arrested in M phase by depletion of Cdc20. When GFP-lacI bound the array, cohesin at 5'lacO was low both before and after *URA3* induction (Figure 1C). The result is consistent with the inability of GFP-lacI to block translocating cohesin complexes. Binding of GFP-FFAT-lacI, on the other hand, increased the level of cohesin at 5'lacO following transcription. This finding serves as a proof-of-principle that large immobile objects block translocation of cohesin complexes in yeast. In *B. subtilis*, tethering a DNA-bound repressor to the plasma membrane similarly blocked translocation of bacterial SMC proteins (34).

135 Large DNA-bound proteins block cohesin translocation

136 To determine if large DNA-bound proteins could similarly block cohesin passage, a series of
137 size-calibrated obstacles was generated by fusing increasing numbers of mCherry to GFP-lacI
138 (Figure 2A-C). This red fluorescent protein is ideally suited as a size standard because it has a
139 compact monomeric structure unlike its tetrameric progenitor, DsRed (35-37). Like GFP-lacI,
140 the mCherry chimeras bind lacO arrays, albeit with reduced efficiency, as demonstrated by
141 weaker GFP foci and higher background nuclear fluorescence (Figure S1).
142
143 Accumulation of cohesin at 5'lacO was measured in M phase-arrested cells following three
144 different *URA3* induction protocols (Figure 2D). In the first, *URA3* was never induced.
145 Accordingly, cohesin levels at 5'lacO remained low and comparable to the cohesin-free control
146 site, which is represented by a dashed line in Figure 2E. In the second protocol, *URA3* was
147 induced following imposition of an M phase arrest. In this case, accumulation of cohesin at
148 5'lacO depended on the identity of the GFP-lacI chimera used (Figure 2C). When GFP-lacI was
149 fused to one or two mCherries, cohesin levels did not rise above the baseline. By contrast, when
150 GFP-lacI was fused to three or four mCherries cohesin accumulated at 5'lacO. To be certain that
151 an aberrant property of mCherry was not responsible, the experiment was repeated with a
152 chimera bearing three copies of monomeric yeGFP in place of the three mCherries. Similar
153 results were obtained (Figure S2). These results indicate that DNA bound proteins of sufficient
154 size block passage of translocating cohesin complexes.
155
156 In the final experimental protocol, *URA3* was induced at the outset of asynchronous growth.
157 Previously we found that a downstream convergently-oriented gene could not block translocation
158 of cohesive complexes in this scenario but the basis for this phenomenon was not understood
159 (32). When *URA3* was induced from the outset here, most of the mCherry chimeras similarly
160 failed to accumulate cohesin at 5'lacO. Some binding, however, was detected when GFP-lacI
161 was fused to four mCherries (Figure 2E). That the timing of transcriptional induction influences
162 the size of an effective obstacle further reinforces the notion that an aberrant property of
163 mCherry is not responsible for blockade. Rather, the data suggests that different sized barriers act
164 as obstacles under different conditions. Additional experiments elaborate on this concept below.
165

166 Trapped cohesin complexes remain cohesive

167 Translocation of cohesin along a single chromatid during loop extrusion or along a pair of
168 chromatids during sister chromatid cohesion could yield the ChIP signals seen thus far. To
169 determine whether the complexes at 5'lacO hold sister chromatids together, we evaluated
170 cohesion of the chromosomal domain bearing the locus. In our strains, target sites for the R site-
171 specific recombinase flank the entire region (Figure 3A). Induction of the recombinase during an
172 M phase arrest generates a pair of DNA circles, one from each sister chromatid. Owing to the
173 bound GFP-lacI chimeras, a single dot of fluorescence appears if the DNA circles are cohesed
174 whereas a pair of dots appears if they are not (Figure S1). *URA3* transcription was induced
175 according to the three protocols described above and cohesion was evaluated at the end of the
176 growth protocol (Figure 3B). In the absence of induction, cohesion of DNA circles was observed
177 in all strains due to the presence of cohesive cohesin on *URA3* (Figure 3C; (32)). When
178 transcription was induced following M phase arrest, cohesion was greatly reduced in strains with
179 chimeras bearing one or two mCherries or none at all. This result indicates that these chimeras
180 are too small to block translocating cohesin. By contrast, cohesion persisted when *URA3*
181 transcription was induced in strains expressing chimeras with three and four mCherries. Thus,
182 consistent with the results in figure 2, DNA-bound chimeras equal to or larger than GFP-lacI-
183 3xmCherry block passage of translocating cohesive cohesin. We conclude that at least some of
184 the trapped cohesin complexes detected by ChIP are engaged in sister chromatid cohesion.
185
186 When transcription was induced from the outset of cell growth, cohesion of the DNA circles was
187 abolished in all strains, irrespective of the chimera expressed. This result recapitulates the earlier
188 observation that convergent genes downstream of *URA3* also do not trap cohesive complexes
189 under identical induction conditions (32). These data suggest that the ability of an obstacle to
190 block passage of cohesin depends on the interplay between transcription and cell cycle stage.
191 Data supporting this view is presented below.
192
193 A larger barrier is required to block cohesin translocation in late G1 phase

194 The studies above examined translocation of cohesin on newly replicated chromatids in M
195 phase-arrested cells. To study translocation on unreplicated chromatin, cells were arrested in late
196 G1 by expressing a non-degradable allele of Sic1, a Cdk1 inhibitor that prevents S phase entry

197 (38). By definition, the chromatin-bound complexes at this stage of the cell cycle are not
198 cohesive. The steps of the growth protocol are depicted in figure 4A and validation of the growth
199 arrest is shown in figure S3. Transcriptional induction of *URA3* following late G1 arrest caused
200 accumulation of cohesin at 5'lacO only in a strain expressing GFP-lacI-4xmCherry. In strains
201 expressing GFP-lacI-3xmCherry or GFP-lacI alone, cohesin accumulation matched the
202 background levels of the uninduced controls (Figure 4B). This data shows that different size
203 barriers are required to block cohesin at different stages of the cell cycle. Whereas three
204 mCherries were enough to block translocation in M phase, at least four mCherries were required
205 in late G1.
206
207 We hypothesized that the four mCherry threshold seen in figure 4B was related to the same
208 threshold seen during M phase arrest after induction from the outset of growth (Figure 2E). To
209 understand this line of reasoning, recall that cohesin binding resets after each anaphase passage
210 when separase activity subsides and Mcd1 synthesis resumes (39-41). If *URA3* is already
211 transcribing when cohesin binding resumes in late G1 then the ensuing translocation of the
212 complex would occur on an unreplicated chromosome, at least until S phase. Put simply,
213 translocation before DNA replication would bypass the three mCherry limitation normally seen
214 in M phase cells. To test this idea, *URA3* was induced from the outset of growth and barrier
215 activity of the obstacles was analyzed by ChIP after cells were arrested in late G1. Figure 4C
216 shows that cohesin accumulated at 5'lacO in transcribing cells that expressed a 4xmCherry
217 obstacle but not the 3xmCherry variant or GFP-lacI alone. These data indicate that when *URA3*
218 is induced from the outset of growth, transcription triggers translocation of cohesin before DNA
219 replication, leading to mobile complexes that pass obstacles the size of GFP-lacI-3xmCherry but
220 not GFP-lacI-4xmCherry.
221
222 <u>Translocation of complexes that arrive after DNA replication</u>
223 Cohesin loads continuously onto chromosomes from late G1 to anaphase (18, 32, 42).
224 Complexes that arrive after DNA replication fail to acquire S phase-dependent acetylation and
225 are turned over by Wpl1 (43, 44). To analyze the translocation properties of these late arriving
226 complexes, *URA3* transcription was induced while cells were arrested in late G1 and then the
227 cultures were released for growth into a subsequent M phase arrest. ChIP at this stage thus

228 reports on those cohesin complexes migrating to 5'lacO both before and after S phase. Formally,
229 this induction protocol also records translocation events during DNA replication of the gene, a
230 time span that is likely too short to affect the results significantly. The novel arrest-and-release
231 procedure was achieved by inducible clearance of AID-tagged, "non-degradable Sic1", using the
232 auxin analog 1-naphthaleneacetic (Figure S3). The ChIP data of figure 4D show that when *URA3*
233 transcription was induced, cohesin accumulated at 5'lacO in cells that expressed 4xmCherry
234 obstacle but not the 3xmCherry variant or GFP-lacI alone. That the barrier limit does not revert
235 to 3xmCherries indicates that late arriving, non-cohesive cohesin is not blocked by the smaller
236 barrier.
237
238 <u>Eco1 and Wpl1 modulate cohesin's encounters with barriers</u>
239 We next tested the influence of regulators of cohesin, Eco1 and Wpl1, on the ability of the
240 complex to translocate past synthetic obstacles. The proteins were depleted by clearance of AID-
241 tagged alleles during a G1 arrest, then cells were grown to the subsequent M phase arrest before
242 inducing *URA3* (Figures 5A). Validation of protein clearance is shown in figure S4. When Eco1
243 was depleted the smallest obstacle, GFP-lacI alone, blocked cohesin translocation (Figure 5B).
244 This unexpected blockade was dependent on the synthetic barrier: when Eco1 was depleted from
245 a strain lacking GFP-lacI, transcription-dependent accumulation of cohesin at the 5'lacO site was
246 abolished (Figure S5). It appears that Eco1, presumably through acetylation of Smc3, facilitates
247 translocation of cohesin past an array of DNA-bound GFP-lacI.
248
249 To explore the phenomenon further, we examined cohesin translocation in a strain with an *smc1-*
250 *D1164E* allele. This mutation diminishes ATP-hydrolysis by cohesin, creating chromatin-bound
251 complexes that do not require Eco1 for protection against Wpl1 unloading (15, 45, 46).
252 Importantly, this mutation reduces Smc3 acetylation by Eco1 (46). In this strain, *URA3*
253 transcription during an M phase arrest also caused cohesin to accumulate at GFP-lacI alone
254 (Figure 5C). These results reinforce the notion that acetylation of Smc3 by Eco1 influences how
255 cohesin navigates the GFP-lacI array.
256
257 When Wpl1 was depleted, two notable changes occurred. First, depletion of the protein abolished
258 the 3xmCherry barrier, yielding a slight increase in accumulation at the 4xmCherry barrier

259 (Figure 5D). The small signal amplitude may be related to earlier observations that cohesin
260 levels are lower at enrichment sites in the absence of Wpl1 (8, 16, 17). These data suggest that
261 cohesin translocation is less restrained in the absence of Wpl1. The second notable change in
262 figure 5D is that accumulation of cohesin at the 4x chimera occurred even in the absence of
263 *URA3* induction. This feature is not unique to M phase-arrested cells. During late G1 arrest when
264 cohesin accumulates at the 4xmCherry chimera, loss of Wpl1 also eliminated the requirement for
265 *URA3* induction (Figure S6A). Elimination of Wpl1 does not cause mis-regulation of *URA3*
266 transcription. RT-qPCR analysis showed that induction profiles of the gene were relatively
267 unchanged (Figure S4D and S6B). Instead, it seems that basal transcription of *URA3* is sufficient
268 to cause cohesin accumulation at synthetic obstacles in the absence of Wpl1. If cohesin binds
269 less specifically in Wpl1 mutants (47), and the residence time on DNA is longer (43), basal
270 transcription of *URA3* might be sufficient to mobilize mis-targeted complexes toward the
271 synthetic barriers downstream.
272
273 When Eco1 and Wpl1 were co-depleted, cohesin bypassed the 3xmCherry chimera yet the
274 complex was blocked efficiently by the larger 4xmCherry chimera (Figure 5E). Cohesin
275 accumulation did not require *URA3* induction, as seen before when depleting Wpl1 alone.
276 Interestingly, the accumulation of cohesin at GFP-lacI, seen when depleting Eco1 alone, was
277 abolished when both proteins were co-depleted. Apparently, the impact of Wpl1 depletion is
278 dominant when both proteins are absent. Perhaps with a longer DNA residence time conferred by
279 Wpl1 loss, cohesin eventually bypasses GFP-lacI but not the larger GFP-lacI-4xmCherry barrier.
280
281 Interpretation of the cohesin translocation results in the absence of Eco1 and Wpl1 requires
282 knowing the cohesive state of the complexes under study. Thus, we measured cohesion of the
283 *URA3* locus in the absence of the regulators. The experiments were performed without induction
284 of the gene to assess baseline levels of cohesion before mobilization. Depletions were achieved
285 during G1 arrest and then cells were grown to an M phase arrest before DNA circles were
286 excised. As expected, depletion of Eco1 abolished cohesion (Figure 5F). Co-depletion of Eco1
287 and Wpl1 also yielded a severe cohesion defect, as anticipated from earlier work (See (48), and
288 references there in). Wpl1 depletion was previously shown to have an intermediate effect on
289 chromosomal cohesion (16, 17, 48). Here, in the context of a specific chromosomal segment

290 unlinked from flanking genomic sequences, depletion of Wpl1 also abolished cohesion. These
291 data show that the *URA3* locus used in our studies is devoid of cohesive cohesin when Eco1 and
292 or Wpl1 are depleted. Cohesin translocation under these conditions occurs on only one
293 chromatid even though both sisters are present.

294 **Discussion**

295 Despite the intense study of cohesin dynamics and loop formation of chromosomal DNA, few
296 studies have caught cohesin in the act of translocation *in vivo*. Here, we show that synthetic
297 barriers of sufficient size cause ectopic accumulation of the complex downstream of an inducible
298 gene (Figure 2). That a DNA-bound obstacle built entirely of non-yeast proteins blocks the
299 passage of cohesin proves that the complex translocates processively along DNA inside live
300 cells. While our work was underway, a study using nuclease-dead Cas9 as a barrier arrived at a
301 similar conclusion (49). Our study goes further in two significant ways. First, we show that both
302 cohesive and non-cohesive complexes translocate on chromosomes. Second, we show that the
303 two types of complexes are blocked by different size barriers.
304
305 Although transcription triggered translocation in this study, it is not yet clear whether a
306 transcribing polymerase is required once the complex gains mobility. Both ATP-dependent and
307 independent movement of cohesin on DNA have been described *in vitro* (21-25). In the former
308 case, cohesin translocated while associated with NIPBL (Scc2 in yeast), a cofactor that
309 stimulates the ATPase activity of the complex (50). Scc2 has also been implicated in cohesin
310 redistribution *in vivo* (50). Further work is required to determine whether NIPBL/Scc2 is
311 required for the processive movement described here.
312
313 Synthetic obstacles of increasing size serve as a molecular ruler of the embrace of cohesin
314 around DNA. Crosslinking studies have defined one large DNA chamber formed by the
315 interactions of core subunits (Smc1, Smc3 and Mcd1), as well as two smaller DNA chambers
316 partitioned from the larger chamber by the engaged heads of the Smc proteins (Figure 6A, (51)).
317 Synthetic obstacles of sufficient size could block transport of DNA through one or more of these
318 chambers. Significant conformational changes are likely to accompany translocation that could
319 narrow the DNA chamber(s) further, as proposed for the related condensin complex (52). Our
320 work now provides an effective upper size limit (measured in mCherries) for cohesin's DNA
321 embrace while translocating on single chromatin fibers and pairs of sister chromatids.
322

323 An exciting and unexpected finding of this study is that the threshold size of an impassible
324 barrier changes depending on cell cycle stage. In late G1 an obstacle bearing four mCherries
325 blocks translocation whereas only three mCherries are needed in M phase (Figures 2 and 4).
326 Chromosomal loops are formed before DNA replication (7, 53), presumably by loop extruding
327 complexes that interact in a pairwise fashion with a given DNA segment. Additional complexes
328 might also translocate at this stage via single interactions with a given DNA segment (24, 54).
329 We propose that one or both of these classes of cohesin complexes are blocked by the
330 4xmCherry threshold during late G1 arrest (Figure 6B). Importantly, during S phase passage a
331 new class of cohesin complexes emerges: one that can translocate while engaged in sister
332 chromatid cohesion (Figure 3). We propose that it is this class of complex, cohesive cohesin, that
333 cannot bypass the 3xmCherry barrier during M phase arrest (Figure 6C). ChIP signals
334 immediately upstream of the lacO array may nevertheless register the accumulation of
335 heterogenous mixture of complexes in M phase because the stalling of a cohesive complex may
336 cause the subsequent accumulation of all others.
337
338 The view that only non-cohesive complexes are trapped by the 4xmCherry barrier is supported
339 by the set of experiments in which *URA3* was induced from the outset of growth. In this
340 protocol, only the 4xmCherry barrier limited cohesin passage, even when examined in M phase-
341 arrested cells that contain cohesive cohesin (Figure 2E and 4C). The inability to trap cohesin
342 with the 3xmCherry barrier can be understood when considering cohesin loading relative to
343 ongoing transcription. During the induction from outset protocol, complexes are triggered to
344 migrate as soon as they begin loading in G1, reaching barriers before becoming cohesive in S
345 phase. Similarly, complexes that load and migrate after S phase during this induction protocol
346 also do so without being cohesive (Figure 4D). Thus, the induction from outset experiments only
347 measure translocation of non-cohesive cohesin. In agreement with the late G1 arrest studies,
348 these complexes are also blocked by the 4xmCherry barrier. Nevertheless, a feature of these
349 experiments remains unresolved. During the induction from outset protocol, complexes that
350 translocate into 4xmCherry barriers early in the cell cycle do not become cohesive as cells
351 progress to an M phase arrest. In other words, complexes that can be detected by ChIP at
352 4xmCherry barriers do not yield cohesion under this induction protocol (Figures 2E and 3C). An

353 intriguing possibility is that complexes arrested at barriers before S phase (perhaps those
354 dedicated to extrusion) do not readily convert to cohesive complexes during S phase passage.
355
356 Both Eco1 and Wpl1 influence the size and distribution of chromosome loops in yeast, as do
357 their homologs in higher eukaryotes (7, 8, 24, 29, 30, 55). Whereas Wpl1 restricts loop size by
358 limiting the residence time and location of cohesin on DNA, Eco1 is thought to restrict loop size
359 through a mechanism(s) independent of cohesion establishment. A simple hypothesis holds that
360 conditions which favor more extensive loop extrusion would also favor translocation past smaller
361 synthetic barriers. Indeed, simultaneous depletion of Eco1 and Wpl1 or just Wpl1 alone
362 increased the threshold size of a barrier in M phase cells from 3xmCherries to 4xmCherries
363 (Figure 5D and 5E). However, by using DNA circularization we showed that the locus under
364 study was devoid of cohesive cohesin in the absence of Eco1 and Wpl1 (Figure 5F). Thus, a
365 simpler explanation may hold: the increase in chimera size from 3xmCherries to 4xmCherries
366 reflects the switch to a barrier limit that applies when only non-cohesive complexes are present.
367 If cohesin only binds single chromatids at *URA3* in the absence of Wpl1 (with or without Eco1),
368 then it is not surprising that the barrier limit matches that for translocation on unreplicated
369 chromosomes in wild-type cells. Despite the presence of sister chromatids the complex
370 translocates on single chromatids under these conditions.
371
372 Lastly, depletion of Eco1 alone yielded an entirely unexpected result: GFP-lacI lacking
373 mCherries was sufficient to impede cohesin passage (Figures 5B and S6). The ChIP signal was
374 highly reproducible, statistically significant, and reliant on GFP-lacI expression. Moreover, the
375 result was reinforced with an *smc1-D1164E* mutant that hinders Smc3 acetylation by Eco1, as
376 well as the intrinsic ATPase of cohesin (Figure 5C). Further work is needed to understand how
377 the acetyltransferase facilitates translocation past the synthetic barriers and whether similar
378 events occur at any natural barriers within chromosomes.
379
380 Maps of mammalian chromosomal loops often contain "stripes" that are thought to be a signature
381 of translocating cohesin complexes (56). A typical stripe encompasses interactions between a
382 loop anchor and the rest of the looped domain, as if a cohesin complex that reaches one loop
383 anchorage point extrudes intervening DNA until reaching the other loop anchorage point. Fine

structure mapping shows that stripes contain embedded dots, possibly from paused translocating cohesin complexes (57). The synthetic barriers described here likely mimic the natural impediments (CTCF and other proteins that bind nucleosome depleted regions) that punctuate and terminate stripe patterns. It is not yet clear, however, whether the trapped complexes in our experiments are stably arrested or merely delayed in their passage. Either way, the data show that cohesin translocates on DNA inside living cells in a manner that would give rise to stripes.

390 **Materials and Methods**

391 *Yeast strains and plasmids*

392 Strains generated for this study were confirmed by PCR and/or DNA sequencing. Strains are
393 listed in Table S2 and primers are listed in Table S1. GFP-lacI with a linked SV40 NLS was
394 expressed from either a single or tandem integration of plasmid pGVH60, as noted in the strain
395 table. These integrants were modified by PCR-mediated gene tagging using multimeric repeats
396 of mCherry in plasmids pMAM12 and pMAM44 or 3xyeGFP(A206R) in plasmid pMAM88.
397 Strains with tandem pGVH60 thus yielded simultaneous expression a GFP-lacI chimera and
398 GFP-lacI alone. Strains co-expressing GFP-lacI/GFP-lacI-mCherry chimeras, however, produced
399 identical results to strains expressing the mCherry chimeras alone (Compare figures 4C and S7).
400 Integrating plasmid pXDA2-FFAT was assembled by in vivo recombination from pAFS144-
401 FFAT and pXRA2 (58). pXDL2-GAL1p-Sic1(4m)-AID*-9xmyc was similarly assembled from
402 pXRL2 (58), pRS306-GAL-Mt-4A-SIC1-HA-HIS6-Act (38) and pKan-AID*-9myc (59). Other
403 genomic AID alleles were constructed by PCR tagging with the 3xmAID-5xflag module in
404 pST1933 (NBRP ID: BYP8880; (60)). OsTir1 was from integrated pTIR5 (*ADH1p-OsTir1-*
405 *CaADH1t,* Thomas Eng thesis, U.C. Berkeley*)* or integrated pMSB27 (*ADH1p-OsTir1*(yeast
406 codon optimized)), which was derived by in vivo recombination from pXRT1 (58) and pMK200
407 (NBRP ID: BYP7569).

408

409 *Cell growth and arrest*

410 To arrest cells in M phase for ChIP, methionine was added (Cf = 2mM) to mid-log cultures
411 grown in SC-met to shut-off *MET3p-cdc20*. After 2.5 hours (roughly 80% of the cells adopted a
412 dumbbell shape), cells were washed twice with water and resuspended in SC media lacking
413 uracil to induce *URA3*. Two hours later the cultures were fixed for ChIP, according to (32). To
414 arrest cells in M phase for analysis of cohesion, cultures were grown in SC-met plus dextrose for
415 6-8 hours and then diluted 200-400 fold into SC-met plus raffinose for overnight growth. When
416 cells reached mid-log the following morning, methionine was added. 150 minutes later, cells
417 were washed twice and resuspended in SC media lacking uracil. Two hours later, galactose was
418 added (Cf = 2%) to induce circularization by the R recombinase. Cells were fixed with
419 paraformaldehyde after two additional hours. To arrest cells for ChIP in late G1, dextrose grown
420 cultures were diluted 200-400 fold into SC-met plus raffinose for overnight growth. When the

421 cultures reached mid-log the following morning, alpha factor was added (Cf = 10 μM), and 90
422 minutes later galactose was added to induce expression of *GAL1p-SIC1(4m)-AID*-9xmyc*. After
423 one additional hour, cultures were washed twice with water and resuspended in SC-met plus
424 galactose and pronase E (Cf = 0.1 mg/ml) to release from pheromone arrest. One hour later, the
425 cells were washed twice and resuspended in galactose lacking methionine and uracil. Two hours
426 later, the cultures were fixed for ChIP. For release from late G1 arrest, cells were grown into the
427 arrest as described above but with the following exceptions. After cells were washed to remove
428 alpha factor, they were resuspended in galactose media that lacked uracil but contained
429 methionine and pronase E. Two hours later, dextrose (Cf = 2%) was added to stop expression of
430 Sic1(4m)-AID*-9xmyc and 1-naphthaleneacetic acid (NAA, Cf = 100 μM) was added to degrade
431 the existing protein. Two hours later when cells accumulated in M phase, cultures were fixed for
432 ChIP. For depletion of the cohesin regulators, strains with the various AID alleles were treated
433 with alpha factor for 90 minutes before adding NAA for 60 additional minutes. After release
434 from alpha factor arrest, cells were resuspended in media containing methionine for arrest in the
435 subsequent M phase. 90 minutes later, cells were washed twice before resuspending with media
436 lacking uracil. Two hours later, cells were fixed for ChIP. For cohesion assays involving protein
437 depletions, cells were grown similarly except that cultures were diluted into SC-met plus
438 raffinose for overnight growth. In addition, galactose was added once cells reached the M phase
439 arrest and cells were fixed two hours later.
440
441 *Other techniques*
442 ChIP, RT-qPCR and fluorescence microscopy were performed as described in (32). For ChIP,
443 the mean and SD of three or more biological replicates are presented, unless specified otherwise.
444 All values were normalized to an unlinked cohesin-bound site (549.7 kb on Chr IV). Statistical
445 significance was determined by pairwise Student's t tests relative to the induced 0x mCherry
446 strain, unless specified otherwise. Immunoblots were probed with anti-GFP (G1544, Sigma),
447 anti-myc (9E10, Roche), anti-mini-AID (M214-3, MBL), anti-Pgk1 (ab113687, Abcam) or anti-
448 Rad23 (from the Madura laboratory), and secondary antibodies (W401B and W402B, Promega).
449 ChIP was performed with anti-TAP and protein A Dynabeads (CAB1001 and 10001D,
450 Invitrogen). A ChemiDoc instrument (BioRad) was used for gel imaging.
451

452 **Acknowledgements**
453 We thank the following individuals for reagents: Jason Brickner (pAFS144-FFAT), Michael
454 Knop (pMAM12, pMAM44 and pMAM88), Kiran Madura (anti-Rad23), Adam Rudner (pTIR5)
455 and Benjamin Rowland (yeast BR423 *smc1-D1164E*). We thank Paul Kraycer for comments on
456 the manuscript. This work was funded by United States Public Health Service Grant NIGMS
457 51402 (to M.R.G.). The Flow Cytometry Core Facility of Robert Wood Johnson Medical School
458 and The Rutgers Cancer Institute of New Jersey is supported by grants from the National Cancer
459 Institute (Grant P30ES005022) and NIH (Grant S10OD026876).
460
461 **Competing Interests**
462 The authors declare that no competing interests exist.
463
464

465 **Figure legends**

466 **Figure 1** – Anchoring DNA to the inner nuclear membrane blocks cohesin translocation. **A)**
467 Schematic of transcription-triggered cohesin translocation and blockage by membrane
468 anchorage. Only one repressor is shown for clarity. NE = nuclear envelope. **B)** Schematic of the
469 locus used to test translocation. Binding of Mcd1 is evaluated at the 5'lacO site immediately
470 upstream of the lacO array. **C)** ChIP of Mcd1-TAP. Strains MSB114 and MRG6947 were
471 arrested in M phase by Cdc20 depletion and then *URA3* transcription was induced. Values were
472 normalized to a cohesin bound site (see Materials and Methods). Measurements at a cohesin-free
473 site (534 kb on Chr IV) were averaged for all experiments of the figure panel and shown as a
474 dashed line. p values for pairwise Student's t tests are presented relative to benchmark sample
475 (designated with a dash). ns, not significant.

476

477 **Figure 2** – Synthetic barriers of sufficient size block cohesin translocation. **A**) Schematic of
478 transcription-triggered cohesin translocation and blockage by GFP-lacI chimeras. **B**)
479 Organization of the GFP-lacI chimeras with mCherries. **C**) Immunoblot of GFP-lacI chimeras.
480 Strains expressing MSB174, MSB179, MSB180, MSB181 and MRG7102 were used. The lower
481 molecular weight bands marked with * likely represent partial proteolytic cleavage of mCherry
482 (61). **D**) Experimental flow chart. Transcription was either induced from the outset of growth,
483 after M phase arrest or not at all. **E**) ChIP of Mcd1-TAP. Cohesin binding at the 5'lacO site was
484 evaluated in strains MSB114, MRG6810, MRG6812, MSB165.1 and MRG7060.

485

486 **Figure 3** – Synthetic barriers of sufficient size block translocation of cohesive cohesin. **A**) An
487 assay for cohesion at a specific chromosomal location. The GFP-tagged region of interest is
488 converted to extrachromosomal circles by site specific recombination. Half-filled boxes
489 represent target sites for the inducible R recombinase. **B)** Experimental flow chart. **C**) Cohesion
490 analysis of extrachromosomal circles. Strains MSB35.2, MRG6806, MRG6808, MSB167 and
491 MRG7060 were used. p values for pairwise $\chi 2$ tests are presented relative to a benchmark
492 condition for each strain (designated with a dash). Error bars represent the standard error of
493 proportion. n = the number of cells examined.

494

495 **Figure 4** – Synthetic barriers to cohesin translocation before and after S phase. **A**) Experimental
496 flow chart. **B**) Barriers to translocation in late G1-arrested cells. ChIP of Mcd1 was performed in
497 strains MRG7027, MRG7026 and MRG7059 that were arrested by expression of non-degradable
498 Sic1. *URA3* transcription was induced after cell cycle arrest. **C**) Same as **B** except transcription
499 was induced from the outset of growth. Two trials were performed for each strain. **D**) Barriers to
500 translocation in cells progressing from G1 to M phase. Details of the cell cycle arrest, release and
501 re-arrest are described in Materials and Methods. Strains MRG7033, MRG7032 and MRG7282
502 were used.
503
504 **Figure 5** – The impact of cohesin regulators on translocation past synthetic barriers. **A**)
505 Experimental flow chart. **B)** Translocation in the absence of Eco1. 3xmAID alleles of Eco1 were
506 depleted by the addition of 100 μM NAA to strains MRG7301.1, MRG7300.1, MRG7302.1, as
507 described in Materials and Methods. p values for pairwise Student's t-tests are presented for the
508 transcriptional induction of each strain. **C)** The impact of *smc1-D1164E* on translocation past
509 barriers. Strains MRG7151, MRG7146 and MRG7159 were arrested in M phase before
510 transcription was induced, as in figure 2. **D)** Translocation in the absence of Wpl1. Strains
511 MRG7327.1, MRG7329.1, MRG7324.1 were used. **E**) Translocation in the absence of Eco1 and
512 Wpl1. Strains MRG7332.1, MRG7356.1, MRG7353.1 were used. **F)** Cohesion of the *URA3*
513 locus in the absence of Eco1 and Wpl1. 3xmAID alleles were depleted during G1 arrest before
514 release into M phase arrest when DNA circles were excised. Strains MSB203, MSB204,
515 MSB205 and MSB206 were used.
516
517 **Figure 6 –** Cohesin translocation blocked by synthetic barriers of sufficient size. **A)** Chambers of
518 cohesin. The large topological compartment created by interactions of Smc3 and Smc1 with
519 Mcd1 is bisected into two smaller chambers by engagement of the Smc3 and Smc1 heads (filled
520 circles, (51)). The chamber(s) used during translocation have not yet been defined. **B** and **C)**
521 Proposed limits of cohesin translocation. Non-cohesive complexes translocating on single
522 chromatids (in late G1 or M phase) cannot translocate past a barrier larger than GFP-4xmCherry.
523 Both loop extruding and singly bound cohesin complexes are depicted. Cohesive complexes
524 during M phase cannot translocate past a barrier larger than GFP-lacI-3xmCherry. Cohesin is
525 represented by a generic ring without reference to chamber(s).

526

527 **Figure S1** – Representative images of cells expressing GFP-lacI chimeras. **A)** Strains MSB35.2,
528 MSB167 and MRG7060 were photographed after M phase arrest. Fluorescent protein chimeras
529 accumulate in the nucleus owing to a C-terminal SV40 NLS. Binding of GFP-lacI alone to the
530 lacO array yielded green foci with little background fluorescence. When chromatids separate,
531 two dots are seen (yellow arrows). Fusion of mCherries to GFP-lacI increases background
532 nuclear fluorescence, suggesting that the C-terminal addition to lacI interferes with chimera
533 binding. Nevertheless, sufficient binding occurs to yield discrete foci. **B)** In the absence of a lacO
534 array (strains MRG7372, MRG7373 and MRG7374), no foci are seen, indicating that GFP-lacI-
535 mCherry chimeras do not intrinsically aggregate.

536

537 **Figure S2 –** GFP-lacI with three copies of yeGFP also blocks cohesin translocation. Strains
538 MSB165.1 and MRG7320 were used. Each of the three yeGFP multimers carries the A206R
539 mutation that abolishes weak dimerization of GFP (62). Cultures were grown as described in
540 figure 2. 3x yeGFP(A206R) yields the same result as 3x mCherry, indicating that residual
541 multimerization of mCherry or some other mCherry artifact is not responsible for barrier activity.
542 The requirement for different sized obstacles at different cell cycle stages further indicates that
543 mCherry multimerization is not driving barrier activity in these studies (compare figures 2 and
544 4).

545

546 **Figure S3** – Stepwise cell cycle arrests using controlled expression on "non-degradable" Sic1.
547 **A**) Cell viability following induction and clearance of Sic1(4m)-AID*-9xmyc. Strains bearing a
548 *GAL1p-SIC1(4m)-AID*-9xmyc* allele (MRG7027 and MRG7033) were spotted in 10-fold serial
549 dilutions on the indicated plates. Galactose-induced lethality due to Sic1(4m)-9xmyc-AID*
550 expression is over-ridden by 100 μM 1-naphthaleneacetic acid (NAA), which triggers
551 degradation of AID chimeras by OsTir1. Methionine was omitted from all plates for *MET3p-*
552 *cdc20* expression. **B**) Validation of Sic1(4m) protein expression levels. The same strains were
553 grown according to the arrest and release protocol described in the Materials and Methods. Lanes
554 1 and 5 = asynchronous growth in dextrose; lanes 2 and 6 = initial late G1 arrest in galactose
555 media, one hour after removing alpha factor; lanes 3 and 7 = extended arrest at late G1 in
556 galactose media, three hours after removing alpha factor; lanes 4 and 8 = two hours after adding

557 NAA. Note that the myc-labelled Sic1(4m)-AID* band is cleared in lane 8 allowing this strain to
558 advance to an M phase arrest. **C**) Validation of late G1 arrest by flow cytometry. Strain
559 MRG7027 was grown into a permanent late G1 arrest as described in Materials and Methods,
560 and used in figure 4B. DNA content was assessed in asynchronous culture, after late G1 arrest
561 and then after subsequent *URA3* induction. **D**) Validation of sequential cell cycle arrests. Top
562 row of panels - Dot plots of flow cytometry data (peak fluorescence vs fluorescence intensity).
563 Strain MRG7033 was used. Cells with clear 1N and 2N DNA content are shown in navy blue
564 and green, respectively. After a prolonged time in late G1 arrest, a large fraction of cells (red)
565 fall outside the gated area due to an elongated bud morphology (due to Sic1-suppressed Cdk
566 activity, (63)) that adversely affects peak fluorescence. Nevertheless, the data show that cells
567 shown in red shift from 1N to 2N DNA content during progression from the late G1 to M arrests.
568 Bottom rows of panels - Direct visualization of cells and cell nuclei. The percentage of cells that
569 meet the specified morphological criteria of each cell cycle arrest are listed below the images.
570 DNA was stained with Hoechst dye after ethanol fixation. n = number of cells examined.
571
572 **Figure S4** – Depletion of cohesin regulators and their impact on *URA3* induction. **A)** Cell
573 viability following depletion of Eco1 and Wpl1. Strains MRG7270.1, MRG7301.1, MRG7327.1,
574 MRG7332.1 and MRG7355.1 bearing the indicated 3xmAID alleles were spotted in 10-fold
575 serial dilutions on SD +leu,+his plates containing or lacking 100 μM NAA. Depletion of Eco1
576 causes a loss of viability that is rescued by co-depletion of Wpl1. Similar results were obtained
577 whether Wpl1 was depleted or the *WPL1* gene was deleted, indicating that depletion phenocopies
578 the null mutation. **B)** Camptothecin sensitivity following Wpl1 depletion. Strains MRG7269.1,
579 MRG7329 (isolate 1), MRG7329 (isolate 2) and MRG6830.1 were spotted on SC-met containing
580 or lacking 20 μg/ml camptothecin (CPT) and 100 μM NAA in 5-fold serial dilutions. Strains
581 lacking Wpl1 are sensitive to the DNA damaging agent (See (47) and references therein). The
582 middle panel shows that addition of the 3xmAID slightly diminishes the function of Wpl1 and
583 the right panel shows that depletion of the protein with NAA phenocopies the null mutation. **C)**
584 Depletion of 3xmAID-tagged proteins. Strains MRG7301.1, MRG7327.1, and MRG7332.1 were
585 used. Cells were grown to mid-log in SC-met and treated with either 100 μM NAA or DMSO for
586 60 minutes. The tagged proteins were immunoblotted with an antibody to mAID. **D)** RT-qPCR
587 analysis of *URA3* mRNA following depletion of mAID-tagged proteins. Strains MRG7270.1,

588 MRG7301.1, MRG7327.1, and MRG7332.1 were grown according to the protocol described in
589 figure 5A. Transcript levels were measured relative to *ACT1* mRNA and normalized to a single
590 trial of the uninduced wt control. The data show that loss of Wpl1 and or Eco1 does not induce
591 *URA3* prematurely.
592
593 **Figure S5** – Barrier activity requires GFP-lacI chimeras. Strain MSB200 (expressing no GFP-
594 lacI chimera) was grown into an M phase arrest following Eco1 depletion during the preceding
595 G1 arrest. *URA3* was then induced. Omission of a GFP-lacI chimera abolishes transcription-
596 dependent cohesin accumulation at 5'lacO.
597
598 **Figure S6** –A synthetic barrier to cohesin translocation in late G1-arrested *wpl1Δ* cells. **A)** ChIP
599 of Mcd1-TAP. Strains MRG7235.1, MRG7232.1 and MRG7238.1 were grown according to the
600 protocol described in figure 4A. Loss of Wpl1 causes accumulation of cohesin at the 4xmCherry
601 barrier without *URA3* transcriptional induction. **B)** RT-qPCR analysis of *URA3* mRNA levels.
602 Strains MRG7027 and MRG7235.1 were grown asynchronously before RNA extracts were
603 prepared. Values normalized as in figure S4. Loss of Wpl1 does not alter the basal level of *URA3*
604 transcription or the ability to induce the gene.
605
606 **Figure S7** – Barrier activity in strains expressing homogeneous GFP-lacI-mCherry chimeras.
607 *URA3* was induced in strains MRG7115 and MRG7122 after arrest in late G1 by Sic1(4m)-
608 AID*-9xmyc. Binding of cohesin at the 5'lacO was analyzed by ChIP of Mcd1-TAP. Barrier
609 function requires 4x mCherries, similar to the results found with strains co-expressing GFP-lacI-
610 mCherry chimeras along with GFP-lacI alone in figure 4.

611 **References**

612 1. Yatskevich S, Rhodes J, & Nasmyth K (2019) Organization of chromosomal DNA by
613 SMC complexes. *Annu Rev Genet* 53:445-482.
614 2. Remeseiro S, Cuadrado A, & Losada A (2013) Cohesin in development and disease.
615 *Development* 140(18):3715-3718.
616 3. Haering CH, Farcas AM, Arumugam P, Metson J, & Nasmyth K (2008) The cohesin ring
617 concatenates sister DNA molecules. *Nature* 454(7202):297-301.
618 4. Lengronne A*, et al.* (2004) Cohesin relocation from sites of chromosomal loading to
619 places of convergent transcription. *Nature* 430(6999):573-578.
620 5. Glynn EF*, et al.* (2004) Genome-wide mapping of the cohesin complex in the yeast
621 *Saccharomyces cerevisiae*. *PLoS Biol* 2(9):e259.
622 6. Schalbetter SA, Fudenberg G, Baxter J, Pollard KS, & Neale MJ (2019) Principles of
623 meiotic chromosome assembly revealed in *S. cerevisiae*. *Nat Commun* 10(1):4795.
624 7. Dauban L*, et al.* (2020) Regulation of cohesin-mediated chromosome folding by Eco1
625 and other partners. *Mol Cell* 77(6):1279-1293.
626 8. Costantino L, Hsieh TS, Lamothe R, Darzacq X, & Koshland D (2020) Cohesin
627 residency determines chromatin loop patterns. *eLife* 9:e59889.
628 9. Oomen ME, Hedger AK, Watts JK, & Dekker J (2020) Detecting chromatin interactions
629 between and along sister chromatids with SisterC. *Nat Methods* 17(10):1002-1009.
630 10. Hadjur S*, et al.* (2009) Cohesins form chromosomal *cis*-interactions at the
631 developmentally regulated *IFNG* locus. *Nature* 460(7253):410-413.
632 11. Rao SSP*, et al.* (2017) Cohesin loss eliminates all loop domains. *Cell* 171(2):305-320
633 e324.
634 12. Mitter M*, et al.* (2020) Conformation of sister chromatids in the replicated human
635 genome. *Nature* 586(7827):139-144.
636 13. Rolef Ben-Shahar T*, et al.* (2008) Eco1-dependent cohesin acetylation during
637 establishment of sister chromatid cohesion. *Science* 321(5888):563-566.
638 14. Ünal E*, et al.* (2008) A molecular determinant for the establishment of sister chromatid
639 cohesion. *Science* 321(5888):566-569.
640 15. Beckouët F*, et al.* (2016) Releasing activity disengages cohesin's Smc3/Scc1 interface in
641 a process blocked by acetylation. *Mol Cell* 61(4):563-574.
642 16. Rowland BD*, et al.* (2009) Building sister chromatid cohesion: Smc3 acetylation
643 counteracts an antiestablishment activity. *Mol Cell* 33(6):763-774.
644 17. Sutani T, Kawaguchi T, Kanno R, Itoh T, & Shirahige K (2009) Budding yeast
645 Wpl1(Rad61)-Pds5 complex counteracts sister chromatid cohesion-establishing reaction.
646 *Curr Biol* 19(6):492-497.
647 18. Lengronne A*, et al.* (2006) Establishment of sister chromatid cohesion at the *S. cerevisiae*
648 replication fork. *Mol Cell* 23(6):787-799.
649 19. D'Ambrosio C*, et al.* (2008) Identification of *cis*-acting sites for condensin loading onto
650 budding yeast chromosomes. *Genes Dev* 22(16):2215-2227.
651 20. Busslinger GA*, et al.* (2017) Cohesin is positioned in mammalian genomes by
652 transcription, CTCF and Wapl. *Nature* 544(7651):503-507.
653 21. Stigler J, Çamdere GO, Koshland DE, & Greene EC (2016) Single-molecule imaging
654 reveals a collapsed conformational state for DNA-bound cohesin. *Cell Rep* 15(5):988-
655 998.

656 22. Davidson IF, *et al.* (2016) Rapid movement and transcriptional re-localization of human
657 cohesin on DNA. *EMBO J* 35(24):2671-2685.
658 23. Kanke M, Tahara E, Huis In't Veld PJ, & Nishiyama T (2016) Cohesin acetylation and
659 Wapl-Pds5 oppositely regulate translocation of cohesin along DNA. *EMBO J*
660 35(24):2686-2698.
661 24. Davidson IF, *et al.* (2019) DNA loop extrusion by human cohesin. *Science*
662 366(6471):1338-1345.
663 25. Kim Y, Shi Z, Zhang H, Finkelstein IJ, & Yu H (2019) Human cohesin compacts DNA
664 by loop extrusion. *Science* 366(6471):1345-1349.
665 26. Sanborn AL, *et al.* (2015) Chromatin extrusion explains key features of loop and domain
666 formation in wild-type and engineered genomes. *Proc Natl Acad Sci U S A*
667 112(47):e6456-6465.
668 27. Fudenberg G, *et al.* (2016) Formation of chromosomal domains by loop extrusion. *Cell*
669 *Rep* 15(9):2038-2049.
670 28. Nasmyth K (2001) Disseminating the genome: joining, resolving, and separating sister
671 chromatids during mitosis and meiosis. *Annu Rev Genet* 35:673-745.
672 29. Wutz G, *et al.* (2017) Topologically associating domains and chromatin loops depend on
673 cohesin and are regulated by CTCF, WAPL, and PDS5 proteins. *EMBO J* 36(24):3573-
674 3599.
675 30. Haarhuis JHI, *et al.* (2017) The cohesin release factor WAPL restricts chromatin loop
676 extension. *Cell* 169(4):693-707.
677 31. Gassler J, *et al.* (2017) A mechanism of cohesin-dependent loop extrusion organizes
678 zygotic genome architecture. *EMBO J* 36(24):3600-3618.
679 32. Borrie MS, Campor JS, Joshi H, & Gartenberg MR (2017) Binding, sliding, and function
680 of cohesin during transcriptional activation. *Proc Natl Acad Sci U S A* 114(7):e1062.
681 33. Brickner JH & Walter P (2004) Gene recruitment of the activated *INO1* locus to the
682 nuclear membrane. *PLoS Biol* 2(11):e342.
683 34. Karaboja X, *et al.* (2021) XerD unloads bacterial SMC complexes at the replication
684 terminus. *Mol Cell* 81(4):756-766.
685 35. Shaner NC, *et al.* (2004) Improved monomeric red, orange and yellow fluorescent
686 proteins derived from *Discosoma* sp. red fluorescent protein. *Nat Biotechnol*
687 22(12):1567-1572.
688 36. Shemiakina, I.I., *et al.* (2012) A monomeric red fluorescent protein with low cytotoxicity.
689 *Nat Commun* 3:1204.
690 37. Shu X, Shaner NC, Yarbrough CA, Tsien RY, & Remington SJ (2006) Novel
691 chromophores and buried charges control color in mFruits. *Biochemistry* 45(32):9639-
692 9647.
693 38. Verma R, *et al.* (1997) Phosphorylation of Sic1p by G1 Cdk required for its degradation
694 and entry into S phase. *Science* 278(5337):455-460.
695 39. Guacci V, Koshland D, & Strunnikov A (1997) A direct link between sister chromatid
696 cohesion and chromosome condensation revealed through the analysis of *MCD1* in *S.*
697 *cerevisiae*. *Cell* 91(1):47-57.
698 40. Michaelis C, Ciosk R, & Nasmyth K (1997) Cohesins: chromosomal proteins that prevent
699 premature separation of sister chromatids. *Cell* 91(1):35-45.
700 41. Hu B, *et al.* (2015) Biological chromodynamics: a general method for measuring protein
701 occupancy across the genome by calibrating ChIP-seq. *Nucleic Acids Res* 43(20):e132.

702 42. Eng T, Guacci V, & Koshland D (2014) ROCC, a conserved region in cohesin's Mcd1
703 subunit, is essential for the proper regulation of the maintenance of cohesion and
704 establishment of condensation. *Mol Biol Cell* 25(16):2351-2364.
705 43. Chan KL*, et al.* (2012) Cohesin's DNA exit gate is distinct from its entrance gate and is
706 regulated by acetylation. *Cell* 150(5):961-974.
707 44. Lopez-Serra L, Lengronne A, Borges V, Kelly G, & Uhlmann F (2013) Budding yeast
708 Wapl controls sister chromatid cohesion maintenance and chromosome condensation.
709 *Curr Biol* 23(1):64-69.
710 45. Çamdere G, Guacci V, Stricklin J, & Koshland D (2015) The ATPases of cohesin
711 interface with regulators to modulate cohesin-mediated DNA tethering. *eLife* 4:e11315.
712 46. Elbatsh AM*, et al.* (2016) Cohesin releases DNA through asymmetric ATPase-driven
713 ring opening. *Mol Cell* 61(4):575-588.
714 47. Bloom MS, Koshland D, & Guacci V (2018) Cohesin function in cohesion, condensation,
715 and DNA repair is regulated by Wpl1p via a common mechanism in *Saccharomyces*
716 *cerevisiae*. *Genetics* 208(1):111-124.
717 48. Guacci V*, et al.* (2015) A novel mechanism for the establishment of sister chromatid
718 cohesion by the ECO1 acetyltransferase. *Mol Biol Cell* 26(1):117-133.
719 49. Zhang Y*, et al.* (2019) The fundamental role of chromatin loop extrusion in physiological
720 V(D)J recombination. *Nature* 573(7775):600-604.
721 50. Petela NJ*, et al.* (2018) Scc2 is a potent activator of cohesin's ATPase that promotes
722 loading by binding Scc1 without Pds5. *Mol Cell* 70(6):1134-1148.
723 51. Collier JE*, et al.* (2020) Transport of DNA within cohesin involves clamping on top of
724 engaged heads by Scc2 and entrapment within the ring by Scc3. *eLife* 9:e59560.
725 52. Ryu JK*, et al.* (2020) The condensin holocomplex cycles dynamically between open and
726 collapsed states. *Nat Struct Mol Biol* 27(12):1134-1141.
727 53. Schalbetter SA*, et al.* (2017) SMC complexes differentially compact mitotic
728 chromosomes according to genomic context. *Nat Cell Biol* 19(9):1071-1080.
729 54. Srinivasan M*, et al.* (2018) The cohesin ring uses its hinge to organize DNA using non-
730 topological as well as topological mechanisms. *Cell* 173(6):1508-1519.
731 55. Wutz G*, et al.* (2020) ESCO1 and CTCF enable formation of long chromatin loops by
732 protecting cohesin(STAG1) from WAPL. *eLife* 9:e52091.
733 56. Vian L*, et al.* (2018) The energetics and physiological impact of cohesin extrusion. *Cell*
734 173(5):1165-1178.
735 57. Krietenstein N*, et al.* (2020) Ultrastructural details of mammalian chromosome
736 architecture. *Mol Cell* 78(3):554-565 e557.
737 58. Chou CC, Patel MT, & Gartenberg MR (2015) A series of conditional shuttle vectors for
738 targeted genomic integration in budding yeast. *FEMS Yeast Res* 15(3):fov010.
739 59. Morawska M & Ulrich HD (2013) An expanded tool kit for the auxin-inducible degron
740 system in budding yeast. *Yeast* 30(9):341-351.
741 60. Tanaka S, Miyazawa-Onami M, Iida T, & Araki H (2015) iAID: an improved auxin-
742 inducible degron system for the construction of a 'tight' conditional mutant in the budding
743 yeast *Saccharomyces cerevisiae*. *Yeast* 32(8):567-581.
744 61. Huang L, Pike D, Sleat DE, Nanda V, & Lobel P (2014) Potential pitfalls and solutions
745 for use of fluorescent fusion proteins to study the lysosome. *PLoS One* 9(2):e88893.

746 62. Zacharias DA, Violin JD, Newton AC, & Tsien RY (2002) Partitioning of lipid-modified
747 monomeric GFPs into membrane microdomains of live cells. *Science* 296(5569):913-
748 916.
749 63. Lew DJ & Reed SI (1993) Morphogenesis in the yeast cell cycle: regulation by Cdc28
750 and cyclins. *J Cell Biol* 120(6):1305-1320.
751

Borrie and Gartenberg, 2021
Figure 1

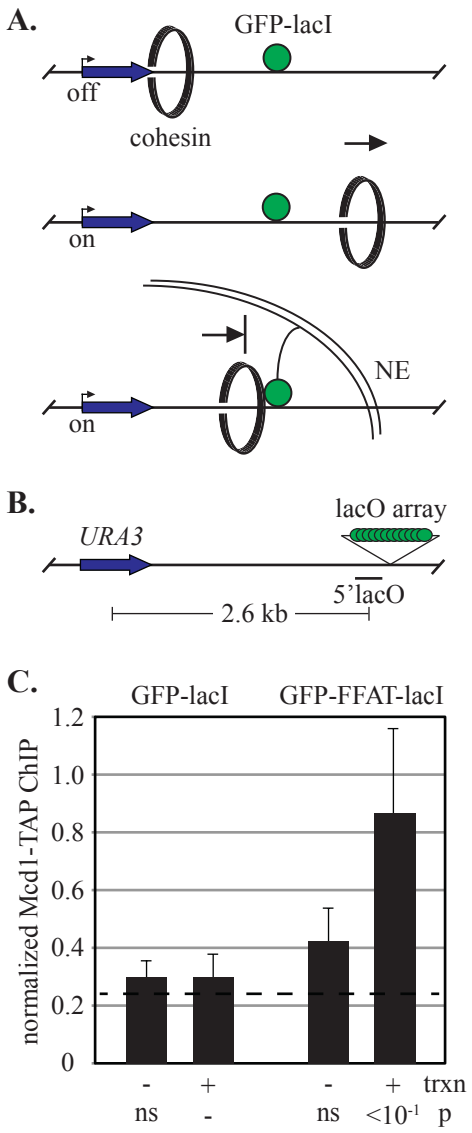

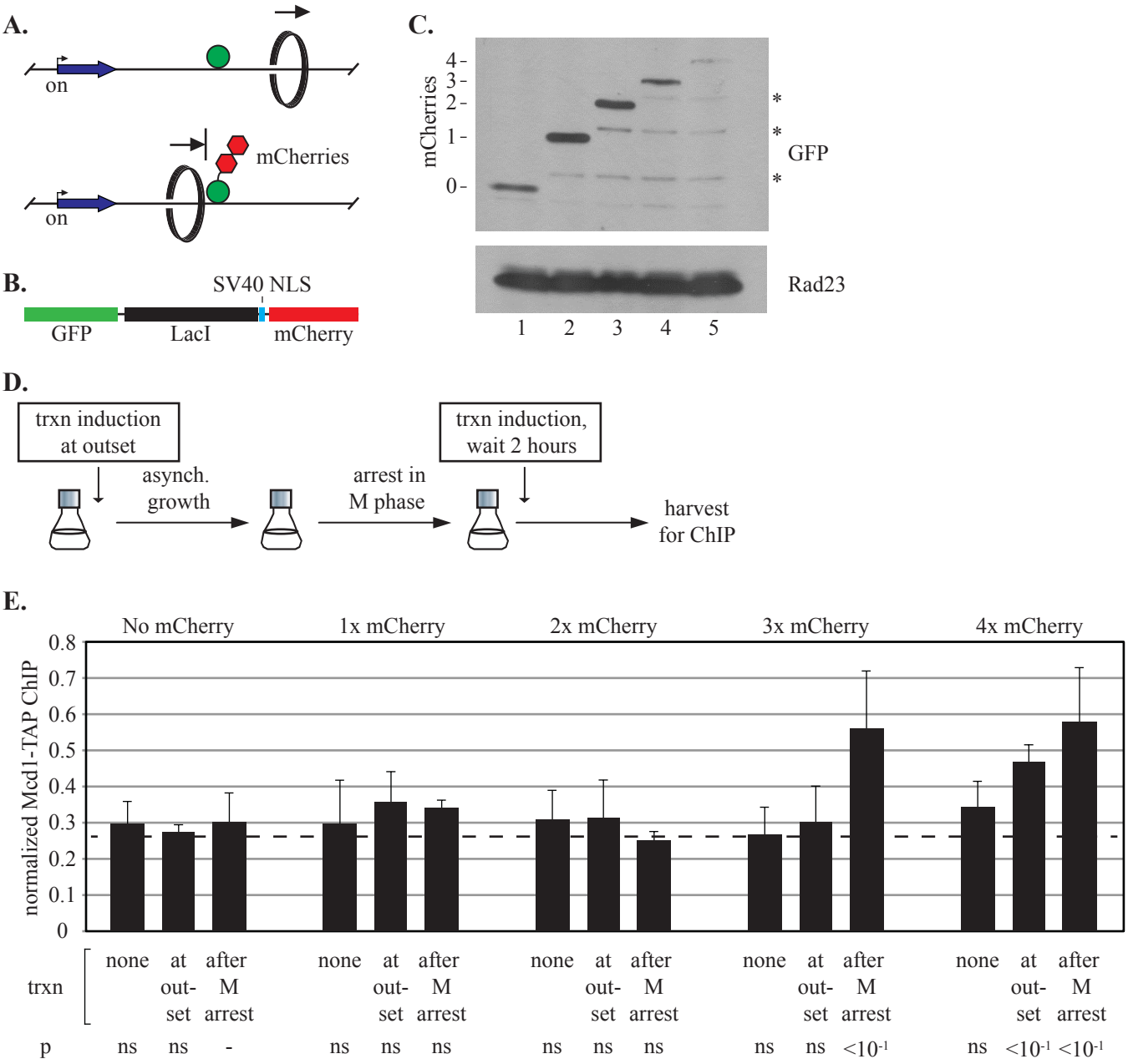
A.
on
mCherries
on
B.
SV40 NLS
GFP
LacI
mCherry
C.
mCherries
4 -
3 -
2 -
1 -
0 -
*
*
*
GFP
Rad23
1 2 3 4 5
D.
trxn induction at outset
asynch. growth
arrest in M phase
trxn induction, wait 2 hours
harvest for ChIP
E.
No mCherry
1x mCherry
2x mCherry
3x mCherry
4x mCherry
normalized Mcd1-TAP ChIP
0.8
0.7
0.6
0.5
0.4
0.3
0.2
0.1
0
trxn
none
at out-set
after M arrest
p
ns
ns
-
ns
ns
ns
ns
ns
ns
ns
ns
<10-1
ns
<10-1
<10-1

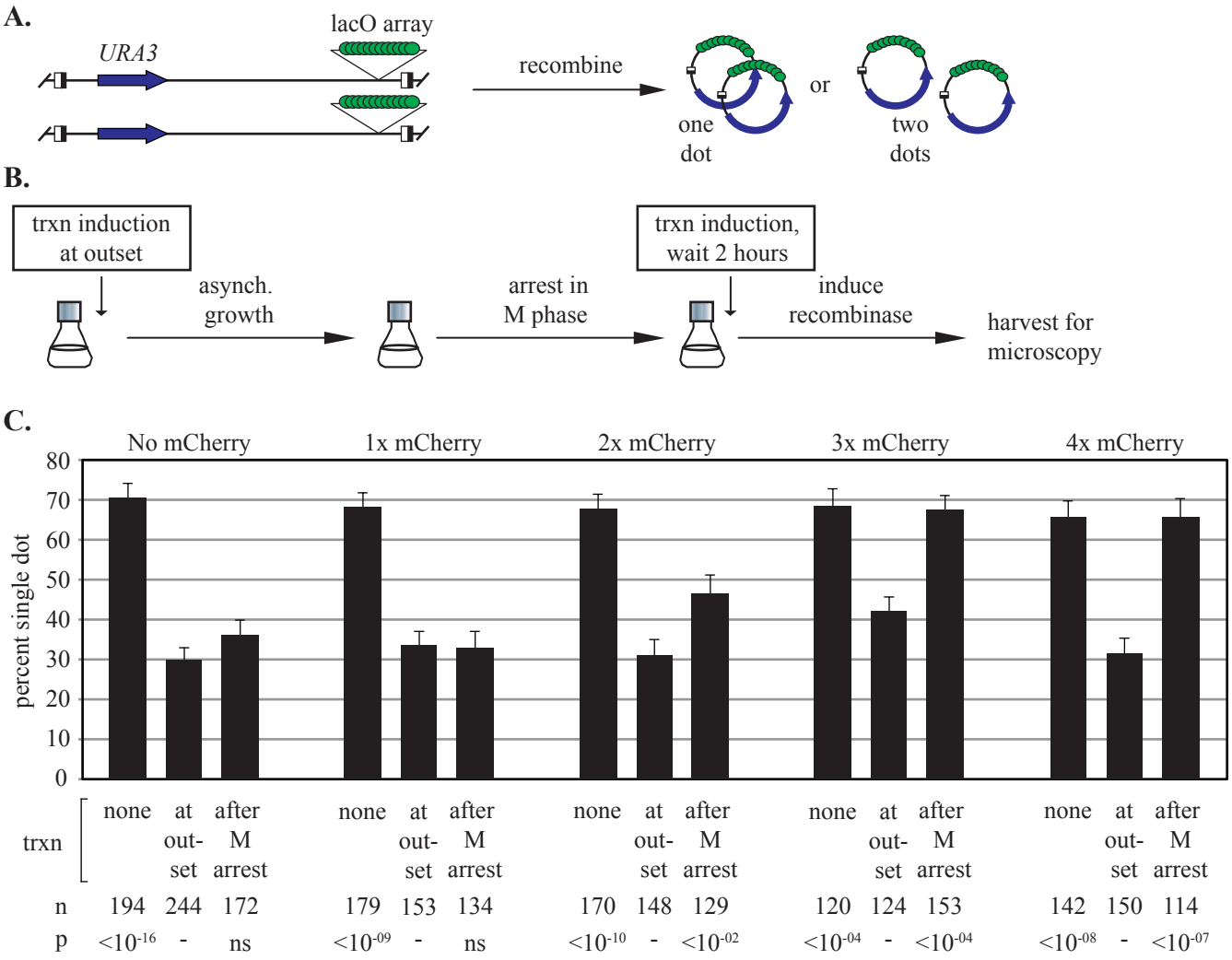
A.
URA3
lacO array
recombine
one dot
or
two dots
B.
trxn induction at outset
asynch. growth
arrest in M phase
trxn induction, wait 2 hours
induce recombinase
harvest for microscopy
C.
No mCherry
1x mCherry
2x mCherry
3x mCherry
4x mCherry
percent single dot
80
70
60
50
40
30
20
10
0
trxn
none
at out-set
after M arrest
n 194 244 172 179 153 134 170 148 129 120 124 153 142 150 114
p <10-16 - ns <10-09 - ns <10-10 - <10-02 <10-04 - <10-04 <10-08 - <10-07

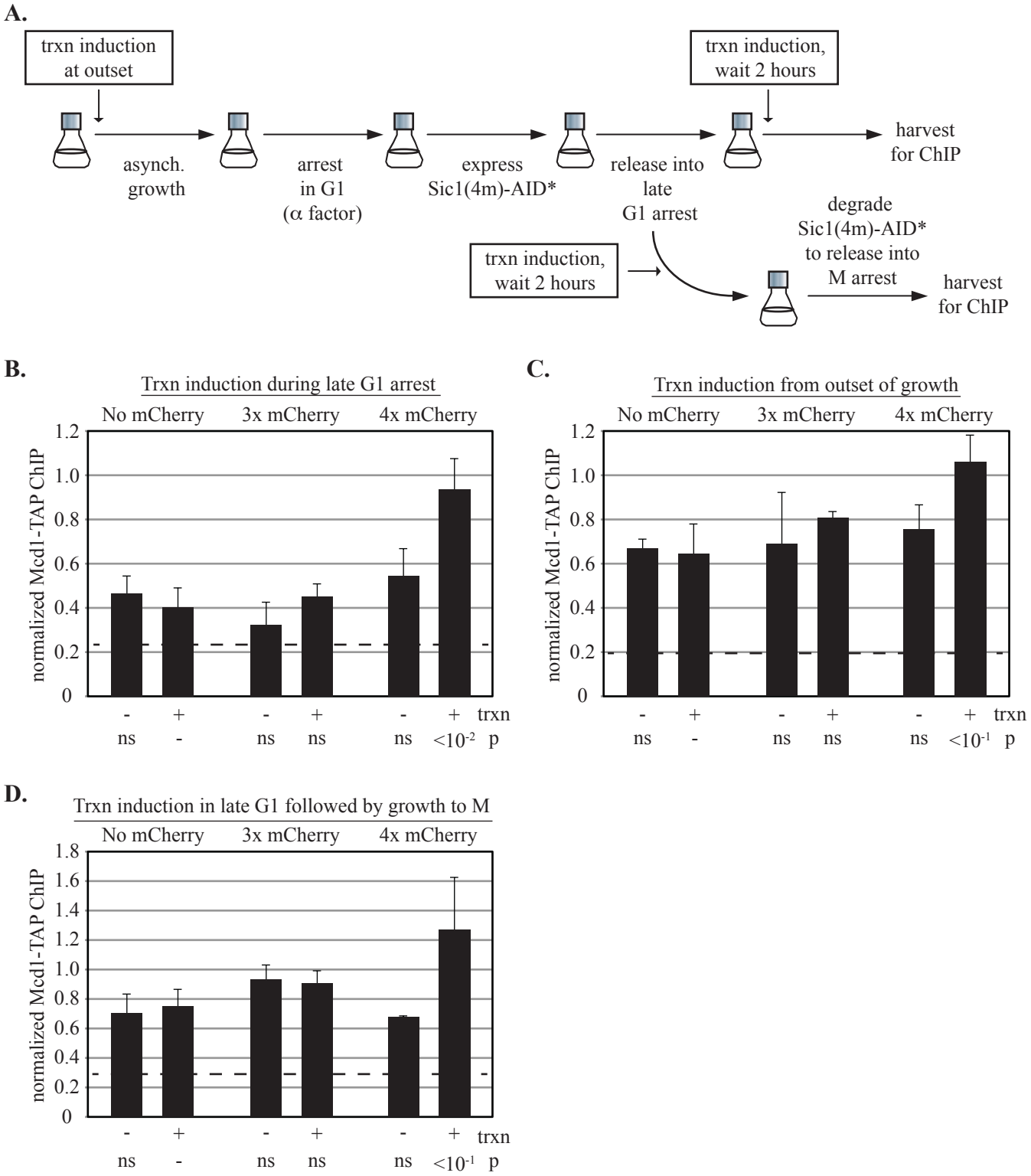
A.
trxn induction at outset
asynch. growth
arrest in G1 (α factor)
express Sic1(4m)-AID*
release into late G1 arrest
trxn induction, wait 2 hours
harvest for ChIP
trxn induction, wait 2 hours
degrade Sic1(4m)-AID* to release into M arrest
harvest for ChIP
B.
Trxn induction during late G1 arrest
No mCherry
3x mCherry
4x mCherry
normalized Mcd1-TAP ChIP
1.2
1.0
0.8
0.6
0.4
0.2
0
- + - + - + trxn
ns - ns ns ns <10-2 p
C.
Trxn induction from outset of growth
No mCherry
3x mCherry
4x mCherry
normalized Mcd1-TAP ChIP
1.2
1.0
0.8
0.6
0.4
0.2
0
- + - + - + trxn
ns - ns ns ns <10-1 p
D.
Trxn induction in late G1 followed by growth to M
No mCherry
3x mCherry
4x mCherry
normalized Mcd1-TAP ChIP
1.8
1.6
1.4
1.2
1.0
0.8
0.6
0.4
0.2
0
- + - + - + trxn
ns - ns ns ns <10-1 p

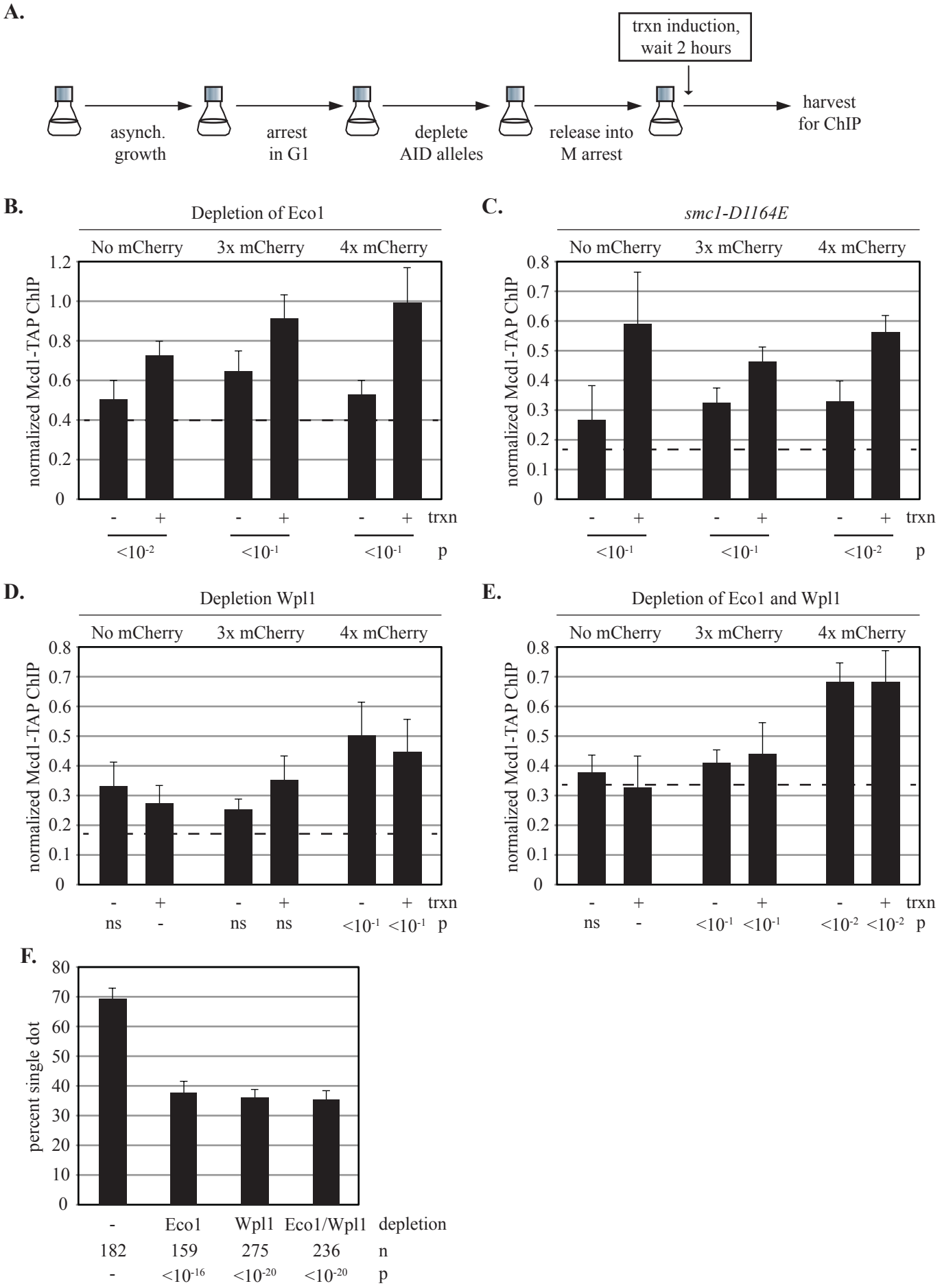
A.
trxn induction, wait 2 hours
asynch. growth
arrest in G1
deplete AID alleles
release into M arrest
harvest for ChIP
B.
Depletion of Eco1
No mCherry
3x mCherry
4x mCherry
normalized Mcd1-TAP ChIP
trxn
p
C.
smc1-D1164E
D.
Depletion Wpl1
E.
Depletion of Eco1 and Wpl1
F.
percent single dot
Eco1
Wpl1
Eco1/Wpl1
depletion
n
182
159
275
236

Borrie and Gartenberg, 2021
Figure 6

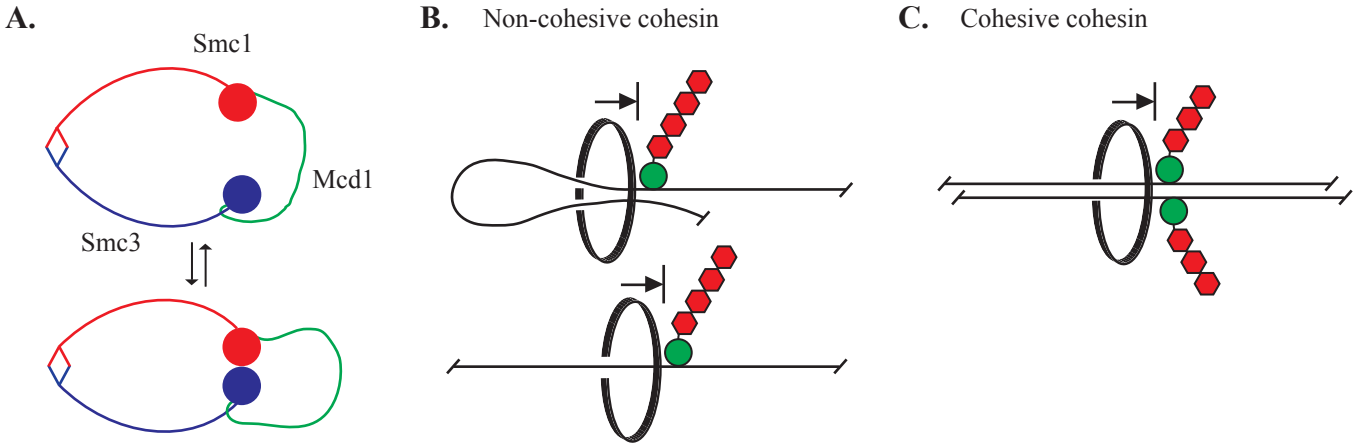

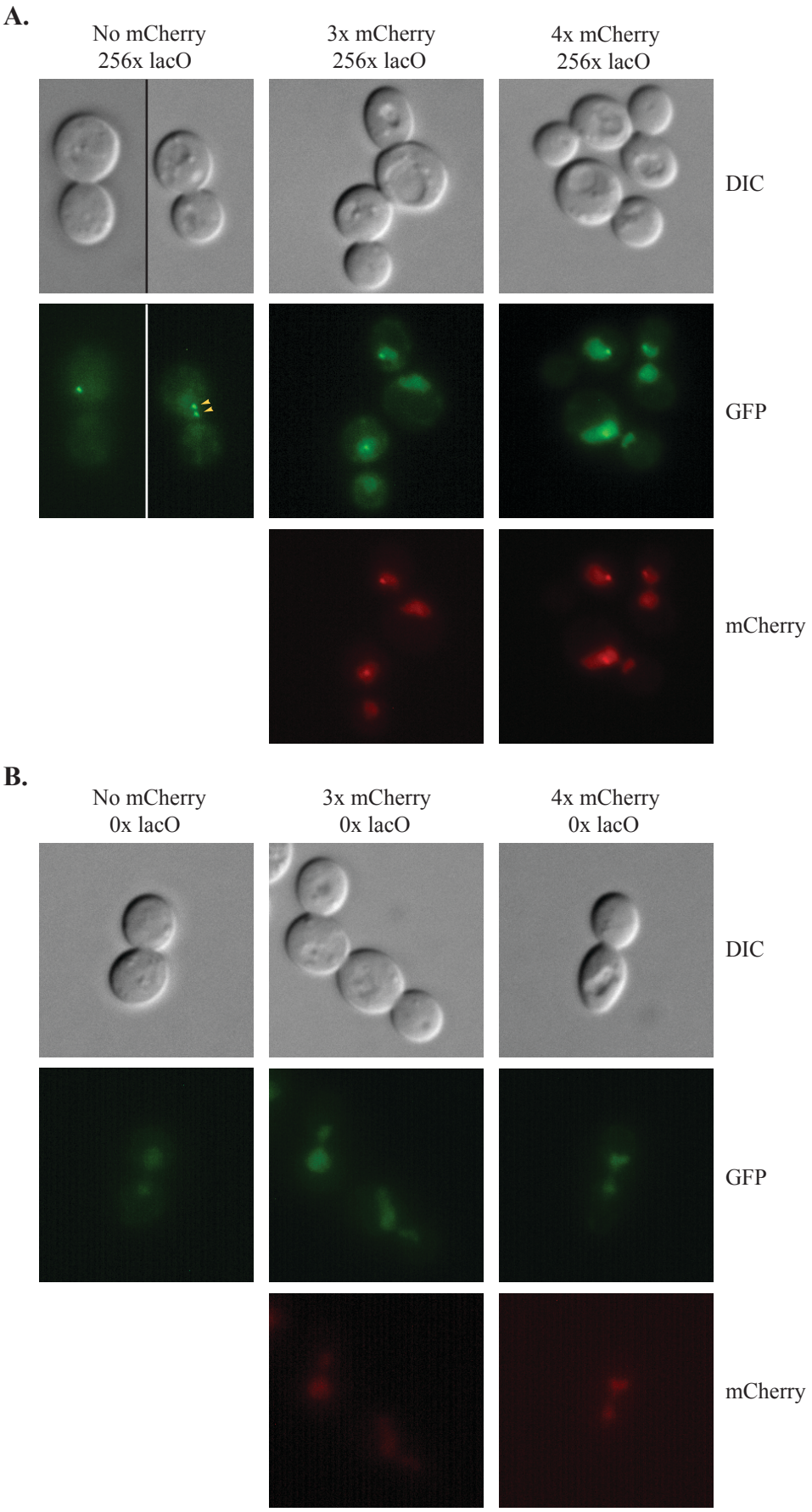
A.
No mCherry
256x lacO
3x mCherry
256x lacO
4x mCherry
256x lacO
DIC
GFP
mCherry
B.
No mCherry
0x lacO
3x mCherry
0x lacO
4x mCherry
0x lacO
DIC
GFP
mCherry

Borrie and Gartenberg, 2021
Figure S2

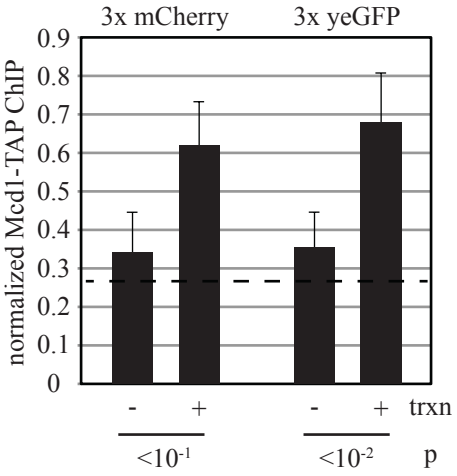

Borrie and Gartenberg, 2021
Figure S3

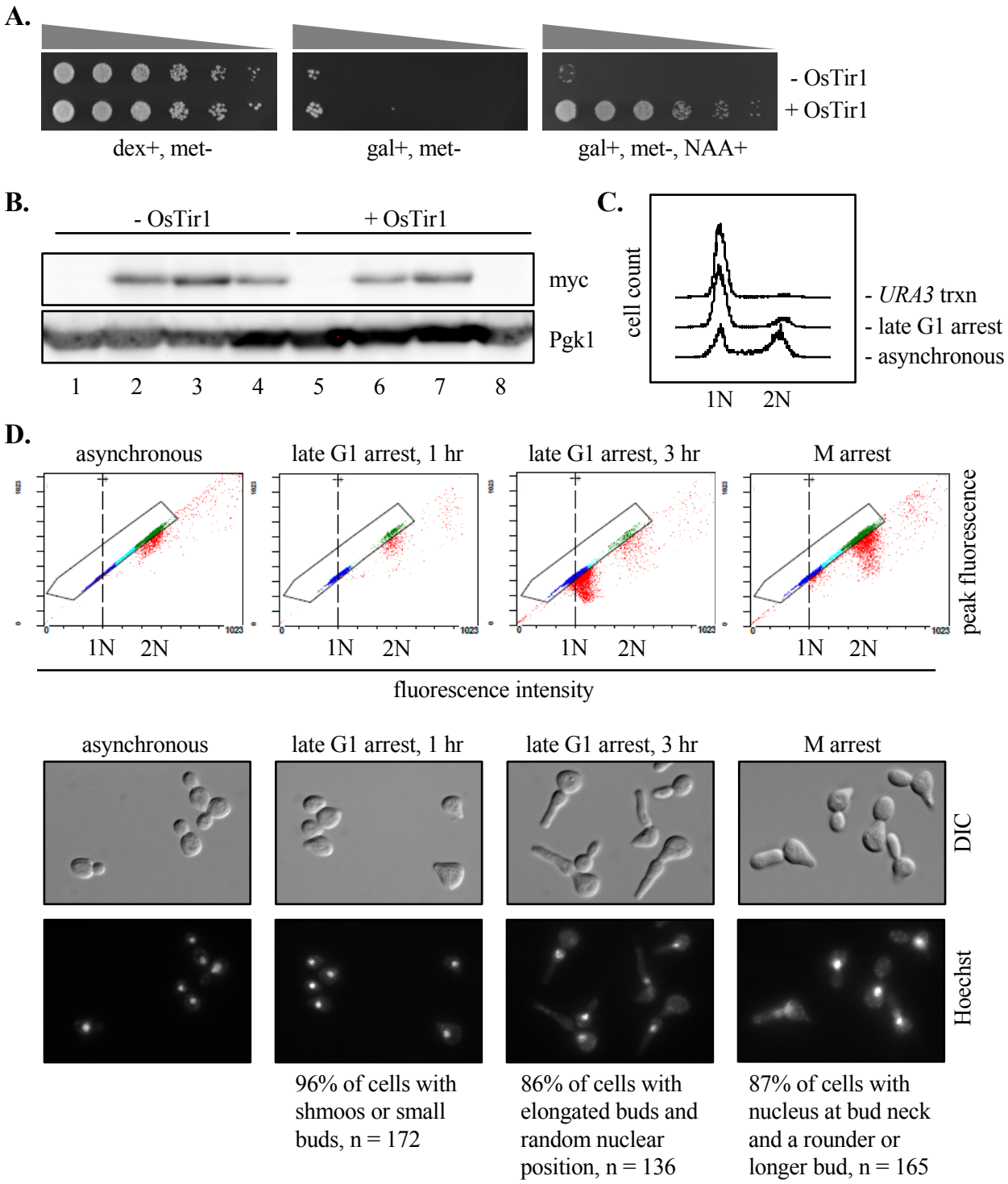

A.

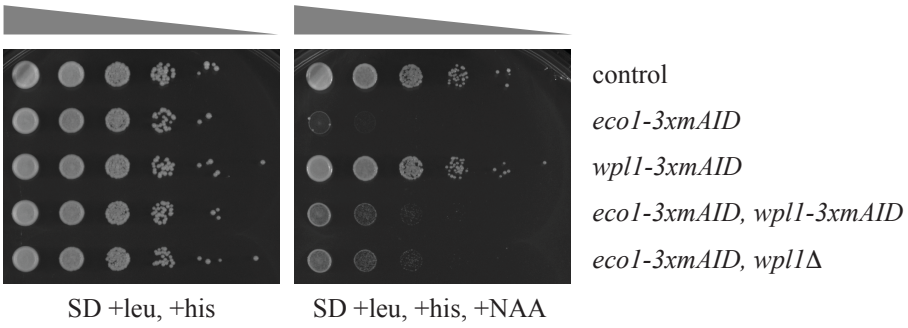
control
eco1-3xmAID
wpl1-3xmAID
eco1-3xmAID, wpl1-3xmAID
eco1-3xmAID, wpl1Δ
SD +leu, +his
SD +leu, +his, +NAA

B.

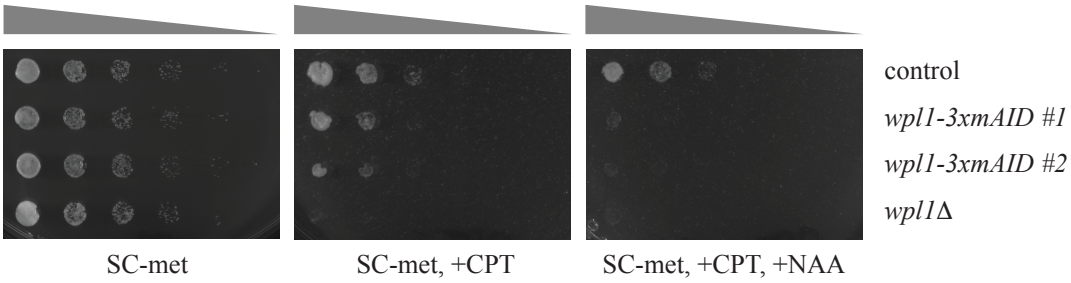
control
wpl1-3xmAID #1
wpl1-3xmAID #2
wpl1Δ
SC-met
SC-met, +CPT
SC-met, +CPT, +NAA

C.

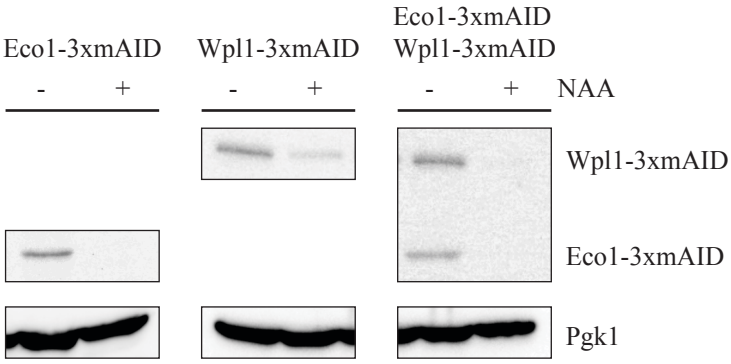
Eco1-3xmAID
Wpl1-3xmAID
Eco1-3xmAID
Wpl1-3xmAID
- +
- +
- +
NAA
Wpl1-3xmAID
Eco1-3xmAID
Pgk1

D.

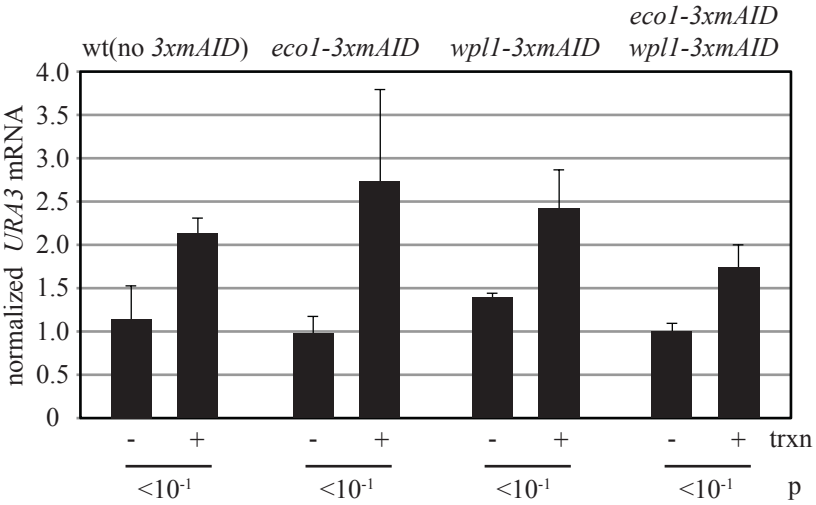
wt(no 3xmAID)
eco1-3xmAID
wpl1-3xmAID
eco1-3xmAID wpl1-3xmAID
normalized URA3 mRNA
4.0
3.5
3.0
2.5
2.0
1.5
1.0
0.5
0
- +
- +
- +
- +
trxn
<10-1
<10-1
<10-1
<10-1
p

Borrie and Gartenberg, 2021
Figure S5

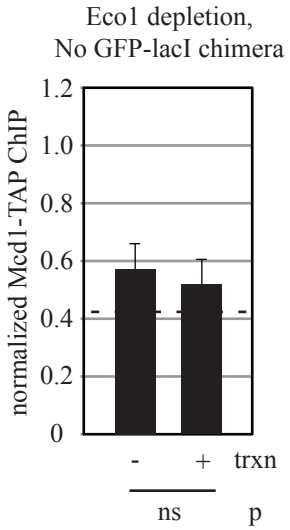

Borrie and Gartenberg, 2021
Figure S6

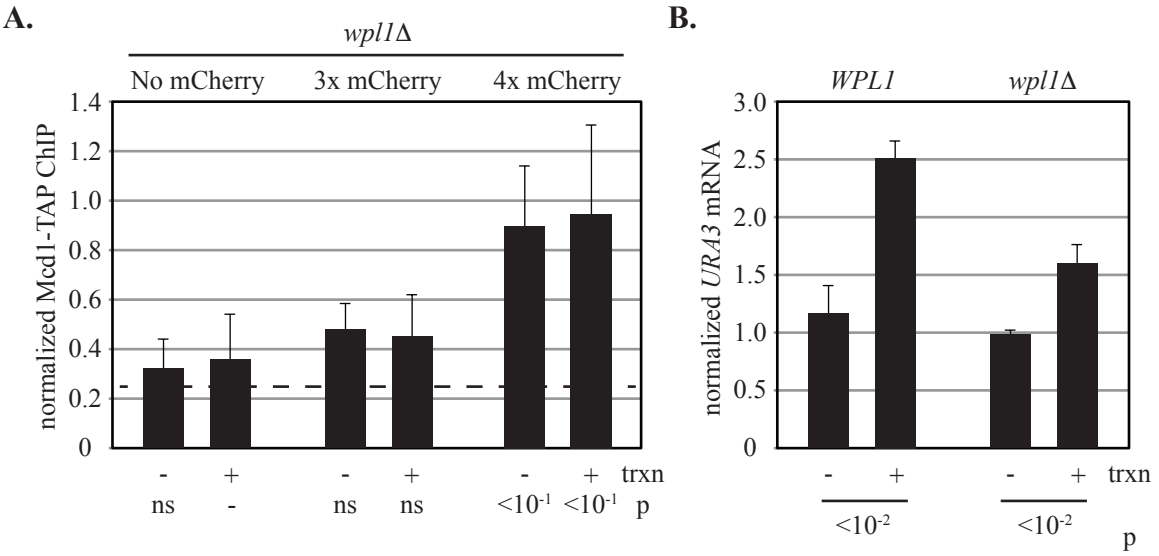
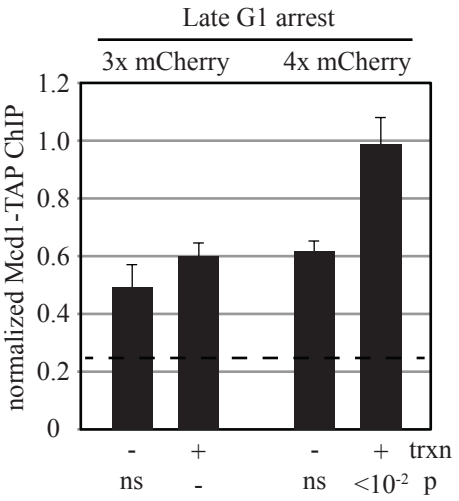
Borrie and Gartenberg, 2021
Figure S7